Splitting of the pygmy dipole resonance in ^{138}Ba and ^{140}Ce observed in the $(\alpha,\alpha'\gamma)$ reaction

J. Endres,[1,*] D. Savran,[2,3] A. M. van den Berg,[3] P. Dendooven,[3] M. Fritzsche,[2] M. N. Harakeh,[3,4] J. Hasper,[1] H. J. Wörtche,[3] and A. Zilges[1]

[1]*Institut für Kernphysik, Universität zu Köln, Zülpicher Straße 77, D-50937 Köln, Germany*

[2]*Institut für Kernphysik, TU Darmstadt, Schlossgartenstrasse 9, D-64289 Darmstadt, Germany*

[3]*Kernfysisch Versneller Instituut, University of Groningen, Zernikelaan 25, NL-9747 AA Groningen, The Netherlands*

[4]*GANIL, CEA/DSM – CNRS/IN2P3, F-14076 Caen, France*

(Received 30 April 2009; published 3 September 2009)

The $N = 82$ nuclei ^{140}Ce and ^{138}Ba have been investigated by means of the $(\alpha,\alpha'\gamma)$ coincidence method to study the pygmy dipole resonance (PDR). The experiments have been performed at the AGOR cyclotron at KVI, Groningen, at a primary beam energy of $E_\alpha = 136$ MeV. The Big-Bite Spectrometer and seven large-volume high-purity germanium detectors were used in coincidence to perform a simultaneous spectroscopy of the scattered α particles and the γ decay. The comparison with results of nuclear resonance fluorescence experiments reveals a splitting of the PDR into two components. Up to about 6 MeV the same states that could be observed in (γ,γ') are also excited in α-scattering experiments, whereas the higher-lying states are missing in the $(\alpha,\alpha'\gamma)$ reaction. This indicates a structural splitting of the PDR into two modes with different underlying structure.

DOI: 10.1103/PhysRevC.80.034302 PACS number(s): 21.10.−k, 24.30.Cz, 25.55.−e, 27.60.+j

I. INTRODUCTION

The $E1$ strength distribution in atomic nuclei is dominated by the isovector giant dipole resonance (IVGDR). In a macroscopic picture this 1 $\hbar\omega$ resonance with angular-momentum change $\Delta L = 1$, isovector character $\Delta T = 1$, and non-spin-flip character $\Delta S = 0$ can be described as a vibration in which the protons and neutrons oscillate out of phase against each other. After the discovery of the IVGDR by Bothe and Gentner [1] and by Migdal, Baldwin, and Klaiber [2,3] and the interpretation by Goldhaber and Teller [4] and Steinwedel and Jensen [5], systematic studies were initiated in the next decade that took advantage of the development of new electron accelerators. Bremsstrahlung has been used to study the resonant γ absorption in nuclei. In addition, experiments with quasimonochromatic photons could be performed by using a tagged-photon beam or e^+e^- annihilation in flight. It was shown that the IVGDR is a collective excitation observed in all nuclei with an excitation energy of $E_x = 31.2A^{-1/3} + 20.6A^{-1/6}$ MeV [6] and a width varying from 2.5 MeV for (spherical) heavy to 5 MeV for light nuclei. Almost 100% of the $E1$ isovector energy-weighted sum rule (IVEWSR) is concentrated in the IVGDR. However, a small fraction of $E1$ strength has been found to be located below the IVGDR. In nuclei near closed shells, the well-known two-phonon $(2^+ \otimes 3^-)_{1^-}$ state is located close to the sum of the energy of the 2^+_1 state and the 3^-_1 state. Furthermore, there is a high concentration of bound 1^- states between 5 and 10 MeV commonly denoted as pygmy dipole resonance (PDR) [7]. The strength of the PDR exhausts about 1% of the IVEWSR and has been studied in many stable nuclei. The most common and well-established method to study the PDR is by means of nuclear resonance fluorescence (NRF) photon-scattering experiments. The electromagnetic interaction of γ rays is well understood, which allows model-independent derivation of absolute transition strengths from such experiments. Because excitations of higher multipolarity are strongly suppressed, dipole excitations become preferred, which makes the NRF method very selective to $E1$ and $M1$ transitions. Using high-purity germanium (HPGe) detectors an excellent energy resolution can be obtained that is necessary considering the high level density even only of the most strongly populated levels of the PDR. Systematic studies, especially in semimagic nuclei, have been performed on the $Z = 82$ nucleus ^{208}Pb [8], on $N = 82$ isotones [9–12], on the $N = 50$ isotones [13–15], and on the $Z = 20$ isotopes ^{40,44,48}Ca [16,17]. Intensive theoretical investigations have been performed in parallel to the experimental programs. An overview is given in the review by Paar *et al.* [18]. Hydrodynamical models have already been used earlier to predict a soft dipole mode as a collective motion of the neutron-rich surface against a core of protons and neutrons [19,20]. This macroscopic picture could also be corroborated in Ca isotopes using the density functional theory formalism [21]. Recent microscopic Hartree-Fock plus RPA calculations with Skyrme effective interactions have studied the isovector dipole response in nuclei with large neutron excess [22–24]. There are several microscopic models that are able to reproduce qualitatively and partly quantitatively the experimental data [17,25–32], although the predicted structure of the wave functions and thus the interpretation of the mode are different.

As mentioned the PDR is often described as an oscillation of a neutron skin against an isospin saturated core. As pointed out by Piekarewicz *et al.* [33], in that case the strength located in the PDR region might provide a possibility to measure the thickness of such a neutron skin. The method has recently been applied to neutron-rich Sn and Sb isotopes via Coulomb excitation of the PDR in inverse kinematics [34].

Despite these efforts, the underlying structure of the PDR is still a matter of ongoing discussion. Additional experimental data are required to improve this situation. Complementary

*endres@ikp.uni-koeln.de

experiments with other probes than photons provide additional observables that may allow a deeper understanding of the PDR. As discussed above, a high selectivity to $E1$ excitations and an excellent energy resolution are mandatory to separate the PDR from other excitations and to perform an analysis of each single state. This implicates strong requirements on the experiment. The pioneering experiments of Poelhekken *et al.* [35] have shown that α-scattering experiments are a powerful tool to study $E1$ transitions by measuring the scattered α particle and the γ decay in coincidence. Poelhekken *et al.* performed $(\alpha,\alpha'\gamma)$ experiments at an incident energy of $E_\alpha = 120$ MeV using a large $10'' \times 14''$ cylindrical NaI γ-ray detector for a few nuclei with rather low level density [35]. The γ-ray energy resolution of about 250 keV at 10 MeV photon energy obtained with the large NaI detector is, however, not sufficient for our purpose. We want to separate the states of the PDR in the semimagic nuclei mentioned above where the spacing of the levels observed in (γ,γ') is only about 10–20 keV. To improve the setup we used the Big-Bite Spectrometer (BBS) at the AGOR facility at KVI for α-particle detection and an array of HPGe detectors for the detection of photons whereby an energy resolution of about 9 keV at 5.5 MeV photon energy could be obtained [36]. We report on the results of the investigations of the PDR with this $(\alpha,\alpha'\gamma)$ method in the two $N = 82$ isotones ^{140}Ce and ^{138}Ba in comparison to results from previous NRF measurements. First results of the ^{140}Ce$(\alpha,\alpha'\gamma)$ experiment have been published recently [37].

II. EXPERIMENTAL SETUP

The AGOR cyclotron was used to produce a 136 MeV α-beam that was guided to the scattering chamber upstream the BBS. This QQD-type spectrometer has a large angular acceptance of up to 13 msr and a K value of 430 MeV and provides the possibility of measuring at scattering angles close to 0° [38]. The light-ion detection system installed at the BBS, the EUROSUPERNOVA (ESN) system, includes two vertical drift chambers (VDCs) and two scintillator planes (S1 and S2). The signals of the latter are used for the α-trigger decision [39]. Each VDC has two wire planes, the X-plane in the vertical direction and the U-plane tilted by 32.9° with respect to the vertical with 240 sense wires each. The VDCs are separated by 230 mm and provide an active detection area of $1030 \times 367\,\text{mm}^2$ each. To determine the position and angles of the scattered α particles in the focal plane the intersection points in the two VDCs are used. This allows the calculation of scattering angle and energy of the scattered α particle.

To detect the subsequent γ-ray emission seven HPGe detectors were positioned with an entrance window distance of about 23 cm to the target. With respect to the beam axis the detectors were positioned at angles between 90° and 150° in the horizontal plane. Each detector has a relative efficiency of about 100% (at $E_\gamma = 1.33$ MeV) compared to a $3'' \times 3''$ cylindrical NaI standard detector. Four detectors were surrounded with bismuth germanate (BGO) shields for active background suppression. The total photopeak efficiency of the array is determined with different radioactive sources with known activities and is about 0.45% at $E_\gamma = 1.33$ MeV and 0.15% at $E_\gamma = 6.0$ MeV. A GEANT4 Monte Carlo simulation [40] has been performed to extrapolate the efficiencies of the single detectors to energies of up to 9 MeV. Therefore, the geometry of the setup has been implemented in the simulation in great detail [36].

A coincidence between signals from the first plane of scintillators and any one of the germanium detectors is requested for the main trigger of the data acquisition, which requires an alignment between the timing of the spectrometer and the HPGe detectors. The suppression of background events is another important issue in this experiment. Because the cross section for elastic scattering at forward scattering angles is several orders of magnitude higher compared to inelastic scattering, the elastically scattered α particles have been blocked physically with an aluminum plate in front of the first VDC. This reduces the count rates due to elastic scattering significantly and random coincidences are suppressed. A second way to reduce the background is to focus the beam on the target instead of using the dispersion-matching mode of the setup. This avoids interaction of the beam α particles with the aluminum target holder that otherwise would produce a high background of γ rays in the germanium detectors. Due to these constraints, the energy resolution of the scattered α particles obtained with the BBS is limited to about 200 keV. The high energy resolution of the germanium detectors can be kept at about 9 keV FWHM at $E_\gamma = 5.5$ MeV in the region of interest. The maximum reasonable count rates in the HPGe detectors of about 15 kHz are the limiting factors of this experiment. To obtain these conditions, the beam current had to be limited to 0.7 pnA for the ^{140}Ce experiment and to 0.9 pnA for the ^{138}Ba experiment. In both experiments, self-supporting metallic targets have been used. In the case of ^{140}Ce the material was isotopically enriched to 99.72%, while for ^{138}Ba the target consisted of naturally composed barium that has a ^{138}Ba content of 71.7%. Both targets showed a contamination by oxygen and hydrogen and in the case of ^{138}Ba also carbon. A summary of the experimental parameters is given in Table I. A detailed description of the experimental setup can be found in Ref. [36].

TABLE I. Experimental parameters for the two measurements.

	^{140}Ce	^{138}Ba
Target thickness (mg/cm^2)	6.8 (7)	7.0 (7)
Isotope enrichment (%)	99.72	71.7
Central BBS angle (°)	3.5	3.5
BBS horizontal opening angle (mrad)	55	55
BBS vertical opening angle (mrad)	105	105
Beam energy (MeV)	136	136
Collected charge (μC)	521	509
Average beam current (pnA)	0.7	0.9
Average γ-trigger rate[a] (kHz)	70	110
Average α-trigger rate[b] (kHz)	14	35
Average coincidence rate[c] (kHz)	0.20	0.86

[a]Defined by the sum of all HPGe detectors.
[b]Defined by the first scintillator plane.
[c]With a coincidence window of $\Delta t = 300$ ns.

III. ANALYSIS

In this section, the data reduction and analysis are presented. In a first step, the γ-ray spectra for ground-state decays are produced for each HPGe detector by applying several constraints to the raw data. From these spectra, differential cross sections for the excitation of single states can be determined.

First, the spectra of the germanium detectors are energy calibrated using a ^{56}Co source. A linear fit is used to extrapolate the calibration to higher energies. The excitation energy, E_x, can be determined by the energy loss, $E_{\rm loss}$, of the α particles. Compared to the energy resolution of the spectrometer the recoil energy of the target nuclei is negligible. The excitation energy can, therefore, be set equal to the energy loss ($E_x \approx E_{\rm loss}$) that is calibrated with known excitations in the target nuclei.

As described in the previous section, elastically scattered α particles are blocked by an aluminum plate in front of the VDCs. This reduces the amount of elastically scattered α particles in the detection system very effectively. Unfortunately, due to scattering at the plate, background events with horizontal angles below 1.55° are produced. Hence, events with a lower horizontal scattering angle are not accounted for in the analysis.

Further random coincidences can be excluded by cutting on the prompt peak in each germanium TDC spectrum. Those timing spectra are produced with respect to the cyclotron frequency of 28.2 MHz. The timing resolution of the prompt peak is about 6 ns FWHM, which is sufficient to separate the prompt peak from random peaks due to the preceding and next beam bursts.

With those conditions, α-γ coincidence matrices can be generated where the γ-decay energy, E_γ, is plotted versus the excitation energy, E_x, (Fig. 1). Transitions between bound states occur in this matrix as thin horizontal lines due to the very good energy resolution of the germanium array compared to the α spectrometer. Different decay channels can be selected by applying cuts on this matrix. Figure 2 demonstrates the selection of ground-state decays. In the upper row, the α-γ coincidence matrix and the total projections onto the x axis (α-spectrum) and the y axis (γ-spectrum) are shown. The latter is dominated by background events even in the high-energy region. In the lower row, the decays to the ground state are selected for the projection by applying the condition of equal excitation and decay energy ($|E_\gamma - E_x| \leqslant 300$ keV). The background is strongly suppressed and the peaks occurring due to ground-state transitions clearly show up in the spectrum. Due to the high resolution, the single peaks are clearly separated and, therefore, an analysis of each single transition is possible.

Depending on the angle of the germanium detector, the α-γ angular correlation produces different relative intensities for transitions of different multipolarities. This angular correlation is calculated with the program ANGCOR [41], which uses the m-state population amplitudes resulting from DWBA calculations, which have been performed using the program CHUCK3 [42,43]. The optical-model parameters needed for the input of CHUCK3 are taken from a global parametrization [44].

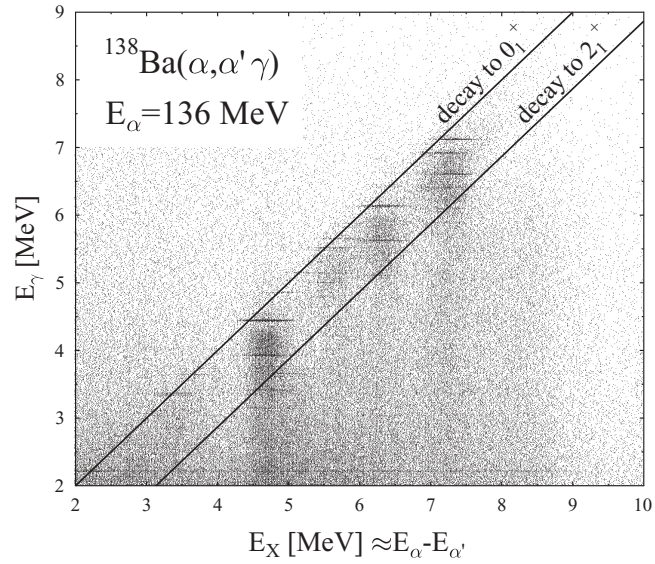

FIG. 1. This α-γ coincidence matrix shows the γ-ray decay energy, E_γ, measured with a germanium detector positioned at backward angles versus the excitation energy, E_x, in the experiment on ^{138}Ba. In this matrix, transitions between bound states occur as thin horizontal lines. The regions of ground-state decays and decays into the 2_1^+ state are marked with diagonal lines.

The point-to-point values of the angular correlation depend on the scattering angles of the α particles and γ rays (θ_α,θ_γ,ϕ_γ) as defined in Fig. 3. The angles θ_γ and θ_α are measured with respect to the beam axis and, therefore, the axis for the angular correlation is also the beam axis. For each germanium detector, the central θ_γ is fixed while a horizontal as well as a vertical opening angle of about $\pm 10°$ is covered. Because of the large acceptance of the BBS an averaging over the values of the angular correlation with respect to θ_α and ϕ_γ for a given θ_γ has to be done. The resulting α-γ angular correlations for different multipolarities are shown in Fig. 4 as a function of θ_γ. Figure 4 shows that the multipolarity of a transition (and, therefore, the spin of the excited state) can be unambiguously assigned by measuring the intensity of the α-γ angular correlation at different angles θ_γ. The accuracy of the calculated α-γ angular correlation has been proven in Ref. [35].

The α-γ angular correlation $W(\Omega_\gamma)$ is also needed to determine the single α-scattering cross section from the double-differential cross section. The relation is given by

$$\frac{d^2\sigma}{d\Omega_\alpha d\Omega_\gamma} = \frac{1}{4\pi}\frac{\Gamma_0}{\Gamma} W(\Omega_\gamma)\frac{d\sigma}{d\Omega_\alpha}, \qquad (1)$$

where the branching ratio $\frac{\Gamma_0}{\Gamma}$ refers to γ decay to the ground state.

In this experiment, the connection between the peak area A_i in one of the germanium detectors and the double-differential cross section is given by:

$$A_i = N_t\, N_\alpha\, \Delta\Omega_\alpha\, \Delta\Omega_{\gamma,i}\, \epsilon_{{\rm int},i}(E_\gamma)\, \Delta_{{\rm live},i}\, \frac{d^2\sigma}{d\Omega_\alpha d\Omega_\gamma}. \qquad (2)$$

In this equation N_t is the number of target nuclei per unit area, N_α the number of incident α particles, $\Delta\Omega_\alpha$ the opening

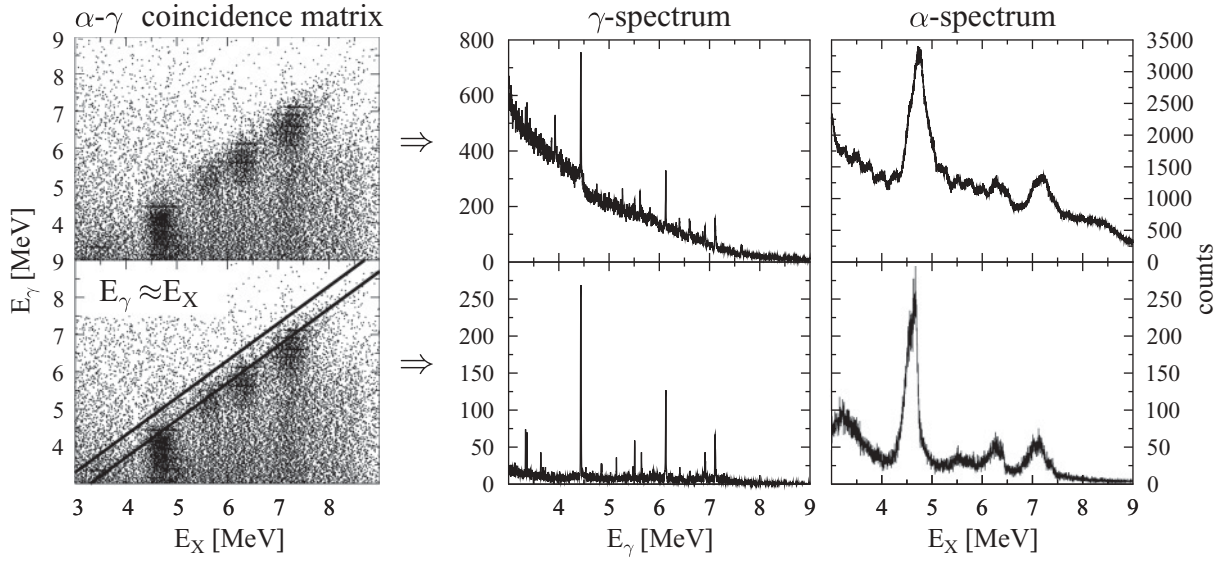

FIG. 2. Two-dimensional scattering matrix and projections for the ^{138}Ba(α,$\alpha'\gamma$) experiment. Different decay channels can be selected by applying conditions on the α-γ coincidence matrix. Ground-state decays can be selected to study $E1$ ground-state transitions of the PDR. The resulting γ spectrum has a strongly reduced background and shows clearly separated peaks.

angle of the spectrometer, $\Delta\Omega_{\gamma,i}$ the opening angle of the ith germanium detector, $\epsilon_{\text{int},i}(E_\gamma)$ the intrinsic efficiency of the ith germanium detector, and $\Delta_{\text{live},i}$ the dead time of the ith germanium detector defined as the ratio between live and measuring time that could be determined with a scaler. Because of low statistics, the spectra of the most efficient and reliable detectors, which were positioned at backward angles, had to be summed up to yield the best peak-to-background ratio. The peak area A is given by the total area F minus the background B.

$$A = F - B \tag{3}$$

For the statistical error of the peak area including the background we assume:

$$\Delta A = \sqrt{A + 2B} \tag{4}$$

The relative uncertainty of the peak area $p = \frac{\Delta A}{A}$ is required to be smaller than $p \leqslant 0.3$ to be accepted in the analysis. To indicate a sensitivity limit the minimal peak area is calculated by

$$A \geqslant \frac{1}{2p^2} + \sqrt{\frac{1}{4p^4} + \frac{2B}{p^2}} \tag{5}$$

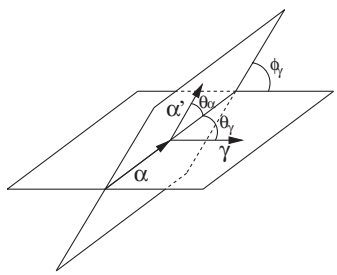

FIG. 3. Illustration of the angles for the α-γ angular correlation.

and can be converted into an energy-dependent cross section sensitivity by using equation (2).

IV. RESULTS AND DISCUSSION

In recent publications [37,45,46], first results for the (α,$\alpha'\gamma$) experiment on the $N = 82$ nucleus ^{140}Ce have already been shown. For the first time, tables of deduced α-scattering cross sections for all observed 1^- states in ^{140}Ce(α,$\alpha'\gamma$) and ^{138}Ba(α,$\alpha'\gamma$) are given in this section. A comparison to the results stemming from NRF experiments by Volz *et al.* [10] will also be given.

From NRF experiments it is known that the states of the PDR predominantly decay into the ground state [9,47,48]. Therefore, the selection of the decay channel into the ground state is an effective filter to separate the states of the PDR from other excitations in the same energy region. Figure 5 shows the decays into the ground state for two different germanium detectors at 202° and 264° for ^{138}Ba(α,$\alpha'\gamma$). The spectra show

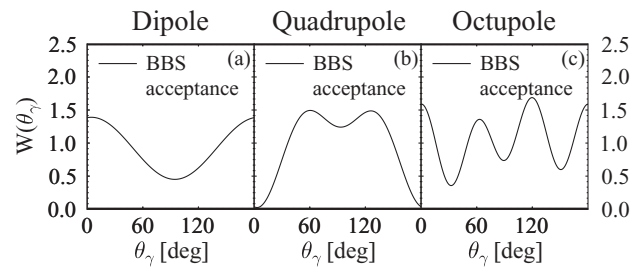

FIG. 4. α-γ angular correlations for transitions from states with $J^\pi = 1^-$, 2^+, and 3^- to the ground state of an even-even nucleus as a function of θ_γ. Each plot shows the distribution of the averaged angular correlation for the full acceptance of the BBS, which was positioned at 3.5°.

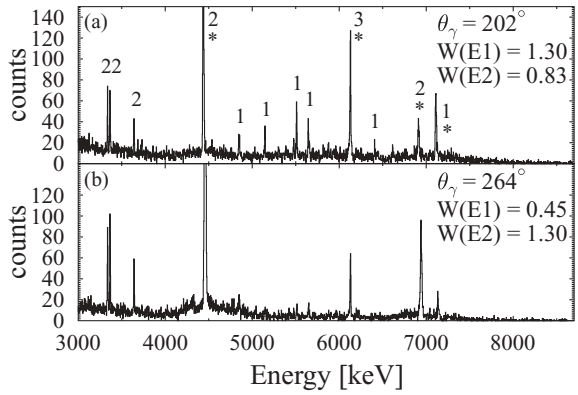

FIG. 5. Ground-state decay spectra obtained with HPGe detectors at different angles for ^{138}Ba($\alpha,\alpha'\gamma$). The value of the averaged angular correlation $W(L\pi)$ is denoted for the corresponding angles. Strong transitions are labeled with the angular momentum. Peaks marked with asterisks (*) stem from background transitions in ^{12}C and ^{16}O.

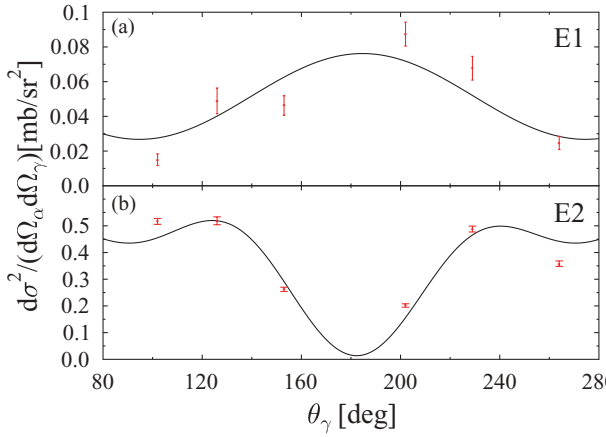

FIG. 6. (Color online) α-γ angular correlations for dipole and quadrupole transitions in ^{138}Ba. The upper plot shows the calculated $E1$ distribution (solid line) and the extracted data points for the 1^- state at 5511.3(10) keV. The lower plot shows the corresponding values for the 2_1^+ state at 1435.816(10) keV. The given errors are statistical only. Due to a laboratory scattering angle of 3.5° (corresponding to the central BBS angle) the angular correlation is not symmetric around 180° and therefore it has been plotted for angles (θ_γ) from 0° up to 360° in the reaction plane.

a very low background and individual peaks are clearly visible. Strong peaks corresponding to known transitions are labeled with their angular momentum. Background peaks stemming from oxygen and carbon contaminations in the target are additionally labeled with an asterisk. Due to the angular correlation $W(\theta)$ (see Fig. 4) transitions with angular momentum $L = 1$ are more intense in the upper spectrum which can, e.g., be seen in the energy region between 5 and 6 MeV. This is a clear sign for electric dipole transitions because only natural parities are excited under the kinematic conditions of the experiment. By comparing these two spectra the multipole character of each observed transition could be identified qualitatively. However, due to low statistics in the single HPGe spectra the angular distribution of the double-differential cross section could be determined only quantitatively for the most prominent peaks. As an example, the angular distributions are shown in Fig. 6 for the 1^- state at 5511.3(10) keV (upper part) and the 2_1^+ state at 1435.816(10) keV (lower part). The energy information and multipole assignment of the transitions allow a secure one-to-one identification between states observed in the ($\alpha,\alpha'\gamma$) and in the (γ,γ') experiments.

In this experiment, no significant branching of the 1^- states into excited states could be observed, which proves that the decay into the ground state is the dominant decay channel. Therefore, $\frac{\Gamma_0}{\Gamma} = 1$ is assumed for the determination of the cross section [see Eq. (2)]. The same assumption has been used in Ref. [10] to extract the $B(E1)\uparrow$ values. However, as many weak (and, therefore, unobserved) branchings to excited states might result in a somewhat smaller $\frac{\Gamma_0}{\Gamma}$, the extracted values for cross sections and $B(E1)\uparrow$ values in both kinds of experiments represent a lower limit. Tables II and III list the single cross sections $\frac{d\sigma}{d\Omega}$ [i.e., after integration of the double-differential cross section over the α-γ angular correlation using Eq. (1)] for the excitation of 1^- states in ^{140}Ce and ^{138}Ba from ($\alpha,\alpha'\gamma$) measurements together with the $B(E1)\uparrow$ values known from NRF. In both tables the errors given for $d\sigma/d\Omega$ are statistical only. For the determination of the absolute values, additional systematic errors have to be taken into account due to the target thickness (10%), the current integration in the Faraday cup (5%), the HPGe efficiencies (5%), and the calculated angular correlation (20%). However, the systematic errors affect all cross sections in the same way and do not influence the relative intensities.

In the upper parts of Figs. 7 and 8, the γ-ray spectra for ground-state decay summed over all the HPGe detectors are shown for the ^{140}Ce($\alpha,\alpha'\gamma$) and ^{138}Ba($\alpha,\alpha'\gamma$) measurements, respectively. In the middle parts of Figs. 7 and 8, the single cross sections determined from the ($\alpha,\alpha'\gamma$) measurement and the corresponding sensitivity limits of the experiment are shown. Finally, the lower parts show the $B(E1)\uparrow$ strength distributions measured in NRF for ^{140}Ce and ^{138}Ba. These

TABLE II. Single cross sections of $E1$ excitations determined from the ^{140}Ce($\alpha,\alpha'\gamma$) measurement and $B(E1)\uparrow$ values from the NRF experiment [10].

Energy (keV)	($\alpha,\alpha'\gamma$) $\frac{d\sigma}{d\Omega}$ (mb/sr)	(γ,γ') $B(E1)\uparrow$ (10^{-3} e^2 fm^2)
3643.8 (6)	0.176 (20)	21.7 (33)
4173.6 (8)	0.140 (19)	5.1 (10)
4514.9 (9)	0.109 (19)	5.3 (10)
4787.8 (9)	0.084 (21)	5.2 (10)
5157.3 (12)	0.116 (25)	3.7 (7)
5190.2 (10)	0.165 (28)	4.6 (9)
5211.6 (14)	0.067 (24)	2.7 (7)
5337.3 (9)	0.347 (37)	4.8 (10)
5548.4 (7)	0.203 (27)	7.9 (14)
5573.8 (14)	0.141 (28)	4.5 (10)
5659.9 (6)	0.341 (35)	26.0 (40)
5928.6 (10)	0.127 (35)	5.4 (11)
6161.7 (14)	0.354 (37)	5.2 (12)

TABLE III. Single cross sections of $E1$ excitations determined from the ^{138}Ba$(\alpha,\alpha'\gamma)$ measurement and $B(E1)\uparrow$ values from the NRF experiment [10].

Energy (keV)	$(\alpha,\alpha'\gamma)$ $\frac{d\sigma}{d\Omega}$ (mb/sr)	(γ,γ') $B(E1)\uparrow$ (10^{-3} e^2 fm^2)
4535.1 (6)	0.080 (7)	5.6 (9)
4854.7 (14)	0.165 (10)	13.1 (20)
5145.4 (6)	0.261 (13)	11.4 (18)
5390.7 (6)	0.128 (10)	12.1 (23)
5475.7 (6)	0.195 (12)	5.5 (9)
5511.3 (10)	0.706 (23)	32.9 (50)
5644.6 (5)	0.428 (18)	24.4 (39)
5655.3 (7)	0.217 (13)	8.6 (18)
5694.5 (7)	0.089 (8)	5.5 (9)
5815.0 (7)	0.125 (10)	6.1 (10)
5873.6 (6)	0.183 (12)	14.7 (23)
5963.5 (6)	0.104 (9)	11.1 (18)
6192.9 (5)	0.096 (9)	21.4 (33)
6410.1 (6)	0.209 (14)	25.7 (40)
6612.7 (6)	0.178 (13)	27.3 (42)
6862.0 (6)	0.110 (10)	15.7 (25)

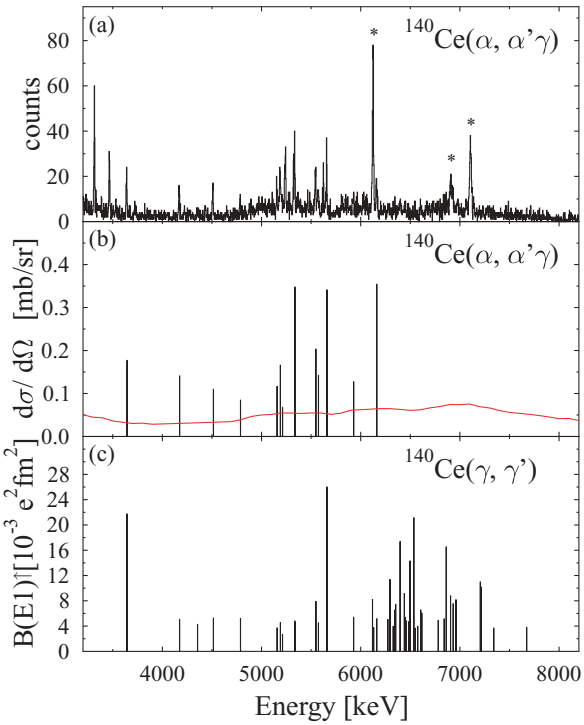

FIG. 7. (Color online) (a) Final γ-ray spectrum for ground-state decay measured in ^{140}Ce$(\alpha,\alpha'\gamma)$ and summed for all the HPGe detectors. Peaks marked with an asterisk (*) stem from transitions in ^{16}O. (b) Single cross sections for the excitation of the 1^- states in ^{140}Ce deduced from $(\alpha,\alpha'\gamma)$ measurement. The solid line shows the energy-dependent sensitivity limit. (c) $B(E1)\uparrow$ strength distribution measured with the (γ,γ') reaction.

spectra are plotted as a function of γ-ray energy, which for γ_0 decay also corresponds to excitation energy. In the case of the $(\alpha,\alpha'\gamma)$ data additional $E1$ transitions might be hidden below the prominent peaks of the strongly first excited states of the carbon and oxygen contamination in the target at 4439, 6130, 6917, and 7117 keV (see spectra in Fig. 5).

Because $B(E1)$ values obtained in NRF experiments and single cross sections measured in $(\alpha,\alpha'\gamma)$ cannot be converted into each other, it is, unfortunately, not possible to compare the absolute values. Nevertheless, in both nuclei, the comparison of the two excitation-energy distributions from $(\alpha,\alpha'\gamma)$ and (γ,γ') show an unexpected behavior. Except for one, all 1^- states below 6 MeV in ^{140}Ce are observed with both methods. Higher-lying 1^- states are not or are much more weakly excited in $(\alpha,\alpha'\gamma)$. Especially the group of strong $E1$ excitations in ^{140}Ce around 6.5 MeV is completely missing. Due to the nearly constant sensitivity limit this effect cannot be explained by a loss of sensitivity. An analog behavior is found in the case of ^{138}Ba. Again up to 6 MeV nearly all 1^- states are excited in both reactions. Only very few weak excitations could be observed in $(\alpha,\alpha'\gamma)$ between 6 and 9 MeV even though the $B(E1)\uparrow$ values of several states are as large as in the lower energy range. This abrupt change of response might be explained by a structural difference between the two groups of 1^- states: A low-energy part that is observed in $(\alpha,\alpha'\gamma)$ as well as in (γ,γ') and a high-energy part that is excited only in (γ,γ'). The states in these two parts of the PDR seem to have different structural characteristics.

Figure 9 shows the $B(E1)\uparrow$ strength distribution convoluted with a Lorentzian shape with $\Gamma = 500$ keV. The gray-shaded distribution shows all 1^- states measured with NRF while the black-shaded distribution includes only states that could be observed with both probes. If a state has been observed in $(\alpha,\alpha'\gamma)$ its full $B(E1)\uparrow$ strength has been considered for the convolution, not considering thereby the values of the cross sections measured in $(\alpha,\alpha'\gamma)$. In the case of ^{140}Ce, there are two concentrations visible that already hint to the existence of two components. The first is located at around 5.5 MeV, and the second at 6.5 MeV. The latter is missing in the $(\alpha,\alpha'\gamma)$ reaction. Also, in ^{138}Ba a concentration around 5.5 MeV is clearly visible in both experiments but the major part around 6.8 MeV is strongly suppressed in $(\alpha,\alpha'\gamma)$, and the concentration of strength at almost 8 MeV is completely missing.

From these results we conclude that the PDR in ^{140}Ce and ^{138}Ba consists of two different components with structurally different states. Two main characteristics of α and γ probes could lead to the selectivity of states. The first is the isospin character, i.e., the α particles are predominantly isoscalar probes at the incident energy of 136 MeV because Coulomb excitation hardly plays a role in the excitation of these states under the experimental condition. However, $E1$ photons excitation is purely isovector. The second is the sensitivity to the radial transition density. The lower-lying states in the PDR might have a large intermediate isoscalar structure, while the higher lying states could be dominantly isovector, which would explain the difference in excitation by both probes. The higher-lying states could be isovector with or without a considerable isoscalar admixture. However, there is a different interaction depth of the two probes with the nucleus. The

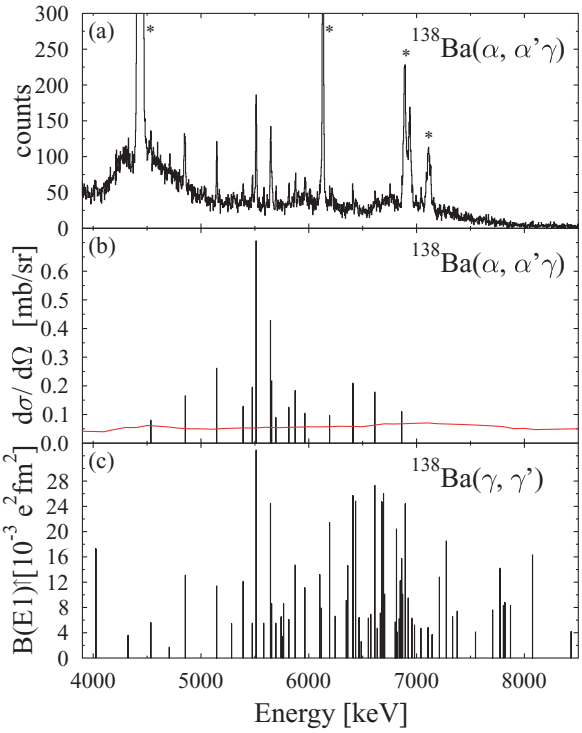

FIG. 8. (Color online) Same as in Fig. 7 but for ^{138}Ba(α,$\alpha'\gamma$) and ^{138}Ba(γ,γ'). Around 4439 keV the spectrum is dominated by the transition stemming from ^{12}C.

electromagnetic field of the photon interacts with the whole nucleus while the α particle interacts at the present bombarding energy mainly with the surface of the nucleus. Therefore, if the higher-lying states also have a large intermediate isoscalar structure with small isospin mixing but with a transition density that is peaked well inside the nuclear surface they could be populated in NRF but not in inelastic α scattering. In such a case of dominant intermediate isoscalar structure, different radial extensions of the involved wave functions might lead to different responses to photons and α particles.

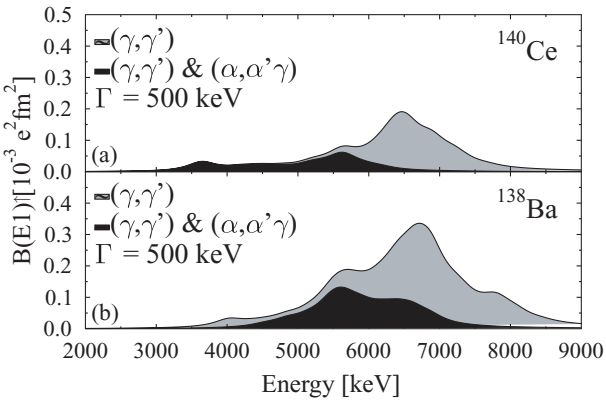

FIG. 9. $B(E1)\uparrow$ strength distribution measured in (γ,γ') convoluted with a Lorentzian function with $\Gamma = 500$ keV for ^{140}Ce (upper part) and ^{138}Ba (lower part), respectively. All of the 1^- states are included in the gray-shaded distribution. The black-shaded distribution includes only states that could be observed in (γ,γ') as well as in (α,$\alpha'\gamma$).

V. SUMMARY AND CONCLUSION

We have investigated the $N = 82$ nuclei ^{140}Ce and ^{138}Ba with the (α,$\alpha'\gamma$) coincidence method. The high selectivity to 1^- states and excellent energy resolution of the experimental method allows a detailed spectroscopy of single states of the PDR.

Cross sections for the excitation of several 1^- states could be extracted from the data and compared to results from (γ,γ') experiments. The comparison between both methods reveals a splitting of the resonance into two energy-separated parts. Almost all states up to about 6 MeV are excited in α scattering, while nearly all higher-lying states are missing in the α-scattering experiment even though the measured $B(E1)\uparrow$ strength is comparable to lower-lying states. This abrupt change points to a splitting of the PDR into two parts with different underlying structure. Because the γ-decay channel into the ground state has been studied in NRF intensively and is therefore well known, the different excitation mechanism due to α scattering must be responsible for the suppression of the excitations above 6 MeV. Different characteristics of the probes are the isospin character and the sensitivity to the radial shape of transition density. The proof has to be delivered that this splitting of the PDR is a common feature and not a special case in $N = 82$ isotones. Therefore, experiments on other nuclei are highly mandatory, for example in the $Z = 50$ and $N = 50$ regions. Because (α,$\alpha'\gamma$) experiments are limited to stable nuclei no direct investigations of unstable nuclei can be performed. Experiments in inverse kinematics with radioactive beams allow the investigation of the PDR in unstable nuclei but suffer from a much lower selectivity and energy resolution. Therefore, an analysis of single states will most probably not be possible. However, an extension of the systematics on the PDR below the particle threshold to exotic nuclei [49] will certainly be of high importance to learn more about this excitation mode of atomic nuclei.

ACKNOWLEDGMENTS

The authors thank S. Brandenburg and the accelerator staff at KVI for their support during the measurement. We thank G. Colò, K. Heyde, F. Iachello, E. Kahn, H. Lenske, J. Leske, V. Yu. Ponomarev, A. Richter, P. Ring, P. von Brentano, and D. Vretenar for stimulating discussions. We further acknowledge the help of M. Elvers, B. Lommel, and S. Müller. This work was supported by the Deutsche Forschungsgemeinschaft (SFB 634 and ZI 510/4-1) and by the LOEWE program of the State of Hesse (Helmholtz International Center for FAIR). The research has further been supported by the EU under EURONS Contract No. RII3-CT-2004-506065 in the 6th framework program.

[1] W. Bothe and W. Gentner, Z. Phys. **71**, 236 (1937).
[2] A. B. Migdal, J. Phys. (Moscow) **8**, 331 (1944).
[3] G. C. Baldwin and G. S. Klaiber, Phys. Rev. **71**, 3 (1947).
[4] M. Goldhaber and E. Teller, Phys. Rev. **74**, 1046 (1948).
[5] H. Steinwedel and J. H. D. Jensen, Phys. Rev. **79**, 1019 (1950).
[6] M. N. Harakeh and A. van der Woude, *Giant Resonances* (Clarendon Press, Oxford, 2001).
[7] G. A. Bartholomew, E. D. Earle, A. J. Ferguson, J. W. Knowles, and M. A. Lone, Adv. Nucl. Phys. **7**, 229 (1973).
[8] N. Ryezayeva, T. Hartmann, Y. Kalmykov, H. Lenske, P. von Neumann-Cosel, V. Y. Ponomarev, A. Richter, A. Shevchenko, S. Volz, and J. Wambach, Phys. Rev. Lett. **89**, 272502 (2002).
[9] D. Savran, M. Fritzsche, J. Hasper, K. Lindenberg, S. Müller, V. Y. Ponomarev, K. Sonnabend, and A. Zilges, Phys. Rev. Lett. **100**, 232501 (2008).
[10] S. Volz, N. Tsoneva, M. Babilon, M. Elvers, J. Hasper, R.-D. Herzberg, H. Lenske, K. Lindenberg, D. Savran, and A. Zilges, Nucl. Phys. **A779**, 1 (2006).
[11] K. Govaert, F. Bauwens, J. Bryssinck, D. De Frenne, E. Jacobs, W. Mondelaers, L. Govor, and V. Y. Ponomarev, Phys. Rev. C **57**, 2229 (1998).
[12] A. Zilges, S. Volz, M. Babilon, T. Hartmann, P. Mohr, and K. Vogt, Phys. Lett. **B542**, 43 (2002).
[13] R. Schwengner, G. Rusev, N. Benouaret, R. Beyer, M. Erhard, E. Grosse, A. R. Junghans, J. Klug, K. Kosev, L. Kostov *et al.*, Phys. Rev. C **76**, 034321 (2007).
[14] R. Schwengner, G. Rusev, N. Tsoneva, N. Benouaret, R. Beyer, M. Erhard, E. Grosse, A. R. Junghans, J. Klug, K. Kosev *et al.*, Phys. Rev. C **78**, 064314 (2008).
[15] N. Benouaret, R. Schwengner, G. Rusev, F. Dönau, R. Beyer, M. Erhard, E. Grosse, A. R. Junghans, K. Kosev, C. Nair *et al.*, Phys. Rev. C **79**, 014303 (2009).
[16] T. Hartmann, J. Enders, P. Mohr, K. Vogt, S. Volz, and A. Zilges, Phys. Rev. C **65**, 034301 (2002).
[17] T. Hartmann, M. Babilon, S. Kamerdzhiev, E. Litvinova, D. Savran, S. Volz, and A. Zilges, Phys. Rev. Lett. **93**, 192501 (2004).
[18] N. Paar, D. Vretenar, E. Khan, and G. Colò, Rep. Prog. Phys. **70**, 691 (2007).
[19] R. Mohan, M. Danos, and L. C. Biedenharn, Phys. Rev. C **3**, 1740 (1971).
[20] Y. Suzuki, K. Ikeda, and H. Sato, Prog. Theor. Phys. **83**, 180 (1990).
[21] J. Chambers, E. Zaremba, J. P. Adams, and B. Castel, Phys. Rev. C **50**, R2671 (1994).
[22] F. Catara, E. G. Lanza, M. A. Nagarajan, and A. Vitturi, Nucl. Phys. **A624**, 449 (1997).
[23] P.-G. Reinhard, Nucl. Phys. **649**, 305c (1999).
[24] A. Vitturi, J. Phys. G **24**, 1439 (1998).
[25] G. Tertychny, V. Tselyaev, S. Kamerdzhiev, F. Grummer, S. Krewald, J. Speth, A. Avdeenkov, and E. Litvinova, Phys. Lett. **B647**, 104 (2007).
[26] G. Colò, N. Van Giai, P. F. Bortignon, and M. R. Quaglia, Phys. Lett. **B485**, 362 (2000).
[27] J. Terasaki and J. Engel, Phys. Rev. C **76**, 044320 (2007).
[28] J. Liang, L. G. Cao, and Z. Y. Ma, Phys. Rev. C **75**, 054320 (2007).
[29] V. Tselyaev, J. Speth, F. Grummer, S. Krewald, A. Avdeenkov, E. Litvinova, and G. Tertychny, Phys. Rev. C **75**, 014315 (2007).
[30] D. Vretenar, A. Wandelt, and P. Ring, Phys. Lett. **B487**, 334 (2000).
[31] D. Vretenar, N. Paar, P. Ring, and T. Nikšić, Phys. Rev. C **65**, 021301(R) (2002).
[32] N. Tsoneva, H. Lenske, and Ch. Stoyanov, Phys. Lett. **B586**, 213 (2004).
[33] J. Piekarewicz, Phys. Rev. C **73**, 044325 (2006).
[34] A. Klimkiewicz, N. Paar, P. Adrich, M. Fallot, K. Boretzky, T. Aumann, D. Cortina-Gil, U. D. Pramanik, T. W. Elze, H. Emling *et al.*, Phys. Rev. C **76**, 051603(R) (2007).
[35] T. D. Poelhekken, S. K. B. Hesmondhalgh, H. J. Hofmann, A. van der Woude, and M. N. Harakeh, Phys. Lett. **B278**, 423 (1992).
[36] D. Savran, A. M. van den Berg, M. N. Harakeh, K. Ramspeck, H. J. Wörtche, and A. Zilges, Nucl. Instrum. Methods A **564**, 267 (2006).
[37] D. Savran, M. Babilon, A. M. van den Berg, M. N. Harakeh, J. Hasper, A. Matic, H. J. Wörtche, and A. Zilges, Phys. Rev. Lett. **97**, 172502 (2006).
[38] A. M. van den Berg, Nucl. Instrum. Methods B **99**, 637 (1995).
[39] H. J. Wörtche (EUROSUPERNOVA Collaboration), Nucl. Phys. **A687**, 321c (2001).
[40] S. Agostinelli, J. Allison, K. Amako, J. Apostolakis, H. Araujo, P. Arce, M. Asai, D. Axen, S. Banerjee, G. Barrand *et al.*, Nucl. Instrum. Methods A **506**, 250 (2003).
[41] M. N. Harakeh and L. W. Put, program ANGCOR, KVI internal report 67i, 1979 (unpublished).
[42] P. D. Kunz, program CHUCK, University of Colorado (unpublished).
[43] J. R. Comfort and M. N. Harakeh, program CHUCK3, modified version of CHUCK, 1979 (unpublished).
[44] M. Nolte, H. Machner, and J. Bojowald, Phys. Rev. C **36**, 1312 (1987).
[45] D. Savran, M. Babilon, A. M. van den Berg, M. N. Harakeh, J. Hasper, H. J. Wörtche, and A. Zilges, Nucl. Phys. **A788**, 165c (2007).
[46] J. Endres, A. Zilges, N. Pietralla, D. Savran, K. Sonnabend, M. N. Harakeh, V. Stoica, H. J. Wörtche, P. Butler, R.-D. Herzberg *et al.*, AIP Conf. Proc. **1090**, 357 (2009).
[47] R.-D. Herzberg, P. von Brentano, J. Eberth, J. Enders, R. Fischer, N. Huxel, T. Klemme, P. von Neumann-Cosel, N. Nicolay, N. Pietralla *et al.*, Phys. Lett. **B390**, 49 (1997).
[48] R. M. Laszewski, Phys. Rev. C **34**, 1114 (1986).
[49] O. Wieland, A. Bracco, F. Camera, G. Benzoni, N. Blasi, S. Brambilla, F. C. L. Crespi, S. Leoni, B. Million, R. Nicolini *et al.* Phys. Rev. Lett. **102**, 092502 (2009).